NEMA NU-04-based Performance Characteristics of the LabPET-8™ Small Animal PET Scanner

Rameshwar Prasad, *Student Member, IEEE*, Osman Ratib, and Habib Zaidi, *Senior Member, IEEE*

***Abstract*– The objective of this study is to characterize the performance of the preclinical avalanche photodiode (APD)-based LabPET-8™ subsystem of the fully integrated trimodality PET/SPECT/CT Triumph™ scanner using the NEMA NU 04 – 2008 protocol. The characterized performance parameters include the spatial resolution, sensitivity, scatter fraction, counts rate performance, and image quality characteristics. The PET system is fully digital using APD-based detector modules with highly integrated electronics. The detector assembly consists of phoswich pairs of LYSO and LGSO crystals with dimensions of 2×2×14 mm^3 having 7.5 cm axial and 10 cm transverse field-of-view (FOV). The spatial resolution and sensitivity were measured using a small ^{22}Na point source at different positions in the scanner's FOV. The scatter fraction and count rate characteristics were measured using a mouse- and rat-sized phantoms fitted with ^{18}F line source. The overall imaging capabilities of the scanner were assessed using the NEMA image quality phantom and laboratory animal studies. The NEMA-based radial and tangential spatial resolution ranged from 1.7 mm at the center of the FOV to 2.59 mm at a radial offset of 2.5 cm and from 1.85 mm at the center of the FOV to 1.76 mm at a radial offset of 2.5 cm, respectively. Iterative reconstruction improved the spatial resolution to 0.84 mm at the center of the FOV. The total absolute system sensitivity is 12.74% for an energy window of 250–650 keV. For the mouse-sized phantom, the peak noise equivalent count rate (NECR) is 183 kcps at 2.07 MBq/cc whereas the peak true count rate is 320 kcps at 2.5 MBq/cc with a scatter fraction of 19%. The rat-sized phantom had a scatter fraction of 31%, with a peak NECR of 67 kcps at 0.23 MBq/cc and a peak true count rate of 186 kcps at 0.27 MBq/cc. The average activity concentration and percentage standard deviation (%STD) are 126.97 kBq/ml and 7%, respectively. The performance of the LabPET-8™ scanner was characterized based on the NEMA NU 04 – 2008 standards. The all in all performance demonstrates that the LabPET-8™ system is able to produce high quality and highly contrasted images in a reasonable time, and as such it is well suited for preclinical molecular imaging-based research.**

***Index Terms*—** PET, instrumentation, small animals, performance evaluation, NEMA.

I. INTRODUCTION

Positron emission tomography (PET) has become an integral non-invasive molecular imaging modality in biomedical and biological imaging research [1]. PET is now a well established imaging modality which has gained widespread clinical acceptance. Moreover, the importance of PET for preclinical imaging has increased manifold during the last decade owing to the capabilities of this technique for studying cellular and molecular processes associated with disease in living small animal models of disease [2]. Clinical whole-body PET scanners are not appropriate for this purpose since they do not provide the high resolution and sensitivity required for small laboratory animal studies [3]. This lead to the design and development of various prototypes dedicated for small animal PET imaging [4-9] resulting in the development of numerous research prototypes as well as several commercially available high-resolution preclinical PET systems [10-14].

The Triumph™ PET/SPECT/CT system (GE healthcare Technologies, Waukesha, WI) is a dedicated trimodality preclinical imaging platform. The scanner consists of the fully digital LabPET™ subsystem [13, 15], cadmium zinc telluride (CZT)-based detectors for the microSPECT subsystem and a high resolution microCT subsystem. All 3 subsystems are mounted on the same gantry offering the possibility to configure the multimodality platform in any combination of the three subsystems. The scanner exhibits several innovative design features rendering it as a high resolution and high sensitive preclinical PET scanner for small animal imaging [13, 15]. Following the widespread use and commercial availability of small animal PET scanners, the National Electrical Manufacturers Association (NEMA) published its NU 4 – 2008 standards [16], a consistent and standardized methodology for measuring scanner performance parameters for small-animal PET imaging. This work aims to characterize the performance of the LabPET-8™ subsystem of the Triumph™ preclinical multimodality platform using the NEMA NU 4 – 2008 standards. This includes measurements of the spatial resolution, scatter fraction, count losses and random coincidence measurements, sensitivity and image quality characteristics. The overall imaging capabilities of the scanner and its suitability for high resolution molecular imaging are also demonstrated using dedicated phantom and rodent studies.

This work was supported by the Swiss National Foundation under grant No. 3152A0-102143.

Rameshwar Prasad is with Division of Nuclear Medicine and Molecular Imaging, Geneva University Hospital, CH-1211 Geneva, Switzerland (e-mail: rameshwar.prasad@unige.ch)

Osman Ratib is with the Division of Nuclear Medicine and Molecular Imaging, Geneva University Hospital, CH-1211 Geneva, Switzerland (e-mail: osman.ratib@hcuge.ch)

Habib Zaidi is with the Division of Nuclear Medicine and Molecular Imaging, Geneva University Hospital CH-1211 Geneva, Switzerland and Department of Nuclear Medicine and Molecular Imaging, University Medical Center, Gronigen, University of Groningen, 9700 RB Groningen, Netherlands (e-mail: habib.zaidi@hcuge.ch).

II. Materials and Methods

A. System description

The Triumph™ PET/SPECT/CT platform is a state-of-the-art preclinical system dedicated for rodents' imaging. The LabPET-8™ subsystem is designed with quasi-individual crystal readout along with parallel digital architecture to achieve the high-performance required for high resolution small animal imaging. The detector array consists of 6144 crystals arranged in contiguous rings with a ring diameter of 16.2 cm and an axial FOV of 7.5 cm. The scintillation crystals are composed of an assembly of $Lu_{0.4}Gd_{1.6}SiO_5$ (LGSO) and $Lu_{1.9}Y_{0.1}SiO_5$ (LYSO) having dimensions of $2\times2\times14$ mm^3, which are optically coupled one after the other, creating phoswich pairs of detectors. Some important characteristics and features of the LabPET-8™ are summarized in Table 1. Additional details about the LabPET-8™ design and architecture is given elsewhere [15, 17].

Table1. Summary of the LabPET-8™ technical specifications.

Parameter	Specification
Detector crystal material	Phoswich pair of LYSO and LGSO
Crystal dimension	$2.0\times2.0\times14$ mm^3
No. of detector rings	32
Crystals per ring	192
Total no. of crystals	6144
Detector ring inner diameter	162 mm
Transaxial field-of-view	100 mm
Axial field-of-view	75 mm

Unless otherwise stated, all PET studies are acquired using a 250–650 keV energy window and 22 ns coincidence timing window. The list-mode data were binned into three-dimensional (3D) histograms or sinograms. These 3D sinograms were further rebinned to two-dimensional (2D) sinograms using single-slice rebinning (SSRB). Images were reconstructed using either 2D analytic filtered-backprojection or iterative maximum likelihood expectation maximization (MLEM) algorithms with 10 iterations for the latter.

The physical response of the scanner fully compensates for the missing data due to in-plane gaps between detector modules. The LabPET-8™ scanner provides the option of image reconstruction in high resolution mode using 0.25 mm pixel size instead of 0.5 mm used in normal mode.

B. Spatial resolution

The spatial resolution was evaluated using a ^{22}Na point source having dimensions of 0.25 mm and an activity of 1.11 MBq enclosed in an acrylic cube of 1 cm^3 (Eckert & Ziegler Isotope Products, Valencia CA). Data were acquired at the center of the FOV (Z=0 mm) and one-fourth of the axial FOV (Z=18.8 mm) for radial offsets of 5 mm, 10 mm, 15 mm, and 25 mm. Each acquisition had more than 10^5 prompt counts. The SSRB sorted data were reconstructed using 2D FBP without smoothing. The spatial resolution in radial, tangential and axial directions was analyzed in terms of full width at half maximum (FWHM) and full width at tenth maximum (FWTM) according to NEMA NU 4 – 2008 standards. Since the scanner design is optimized for iterative reconstruction taking advantage of modeling the system response of the scanner to improve the spatial resolution and overall image quality [18], the spatial resolution was also calculated using 2-D MLEM iterative reconstruction with 10 iterations and span of 5. Both FBP and MLEM reconstructions were performed in high resolution mode. The volumetric resolution was computed as the product of the axial, radial and tangential resolutions.

C. Scatter fraction and counting rate measurements

Scatter fraction and count rate performance were evaluated using specially designed mouse- and rat-sized phantoms according to NEMA NU 4 – 2008 specifications. Both phantoms are made of a solid, circular cylinder composed of high density polyethylene (density 0.96 ± 0.1 g/cm^3). The mouse-sized phantom is 70 ± 0.5 mm long and 25 ± 0.5 mm in diameter whereas the rat-sized phantom has a diameter of 50 ± 0.5 mm and length of 150 ± 0.5 mm. A cylindrical hole (3.2 mm diameter) is bored parallel to the central axis at a radial offset of 10 mm and 17.5 mm for the mouse and rat phantom, respectively. The starting [^{18}F] activity solution is 105 MBq for the mouse-sized phantom and 150 MBq for the rat-sized phantom.To evaluate intrinsic scanner counting rate, two acquisitions of 10 hours each were performed using the mouse and rat phantoms without any radioactivity. For all acquisitions, prompt sinograms without any corrections were generated. Acquisition and processing of data followed strictly the NEMA NU 4 – 2008 standards.

The scatter fraction, count losses and random coincidence analysis was implemented using an in-house developed program implemented in MATLAB 7.4 (Mathworks, Natick, MA).

D. Sensitivity

The sensitivity was measured using the same ^{22}Na point source used in the above described spatial resolution measurements. An acquisition was performed for 10,000 true events by centering the source in the scanner's FOV. The acquisition time was noted and utilized for subsequent acquisitions at positions stepped axially covering the whole scanner's axial FOV. Also the background true event rate was measured by acquiring data in the absence of a radioactive source in the FOV. All data were analyzed according to NEMA NU 4 – 2008 standards.

The axial sensitivity profile was plotted using the absolute sensitivity for each slice.

E. Image quality characteristics

Image quality characteristics were assessed using a specially designed NEMA NU 4 – 2008 image-quality phantom. The

phantom is made up of polymethylmethacrylate with internal dimensions of 50 mm length and 30 mm diameter. The phantom consists of 3 compartments: a uniform region, 5 rods of different diameters and 2 non-radioactive chambers. The phantom was filled with 6.1 MBq of ^{18}F. The acquisition started when the activity in the phantom was 3.7 MBq and lasted 20 minutes. Normalization and random corrections were applied to the acquired data before image reconstruction. The PET emission data were reconstructed using 2D-MLEM (10 iterations, span 63) resulting in a 240×240×63 image matrix with voxel size of 0.25×0.25×1.17 mm^3. A 22.5 mm diameter (75% of active diameter) by 10 mm depth cylindrical volume of interest (VOI) was drawn over the center of the uniform region of the image quality phantom. The average activity concentration, maximum and minimum values in the VOI, and the percentage standard deviation (%STD) were measured. The reconstructed image slices covering the central 10 mm length of the rods were averaged to obtain a single slice of lower noise. Circular ROIs were drawn on this image, around each rod and background, with diameters twice the physical diameter of the rods. The maximum values in each of these ROIs were measured. The transverse image pixel coordinates of the locations with the maximum ROI values were recorded and used to create line profiles along the rods in the axial direction. The standard deviation and mean value of a rod profile and background were calculated. Image quality data were analyzed according to NEMA NU 4 – 2008 standards.

III. RESULTS

A. *Spatial resolution*

The measured radial, tangential and axial spatial resolution in terms of FWHM and FWTM (mm) are plotted in Fig. 1 for FBP reconstruction as recommended by the NEMA NU 4 – 2008 standards. The FWHM radial resolution ranged from 1.7 mm at the centre of the FOV to 2.59 mm at a radial offset of 25 mm whereas the FWTM ranged from 3.1 mm to 4.91 mm for the same radial offset. The axial resolution ranged from 2.41 mm at the centre FOV to 2.63 mm at a radial offset of 25 mm whereas the FWTM ranged from 4.4 mm to 4.79 mm for the same radial offset. The tangential resolution was more or less constant for the radial offsets. The FWHM volumetric resolution at axial positions Z=0 and Z=18.8 mm is 7.5 mm^3 and 8.3 mm^3, respectively.

Iterative reconstruction with accurate statistical modeling of the system's response function improved substantially the spatial resolution. The radial resolution ranged from 0.84 mm at the centre of the FOV to 1.14 mm at a radial offset of 25 mm whereas the FWTM ranged from 1.53 mm to 2.08 mm for the same radial offset. The axial resolution ranged from 1.55 mm at the centre of the FOV to 1.53 mm at a radial offset of 25 mm whereas the FWTM ranged from 2.83 mm to 2.81 mm for the same radial offset. The tangential resolution was almost constant for the radial offsets. The FWHM volumetric resolution at axial positions Z=0 and Z=18.8 mm positions is 1.31 mm^3 and 1.43 mm^3, respectively.

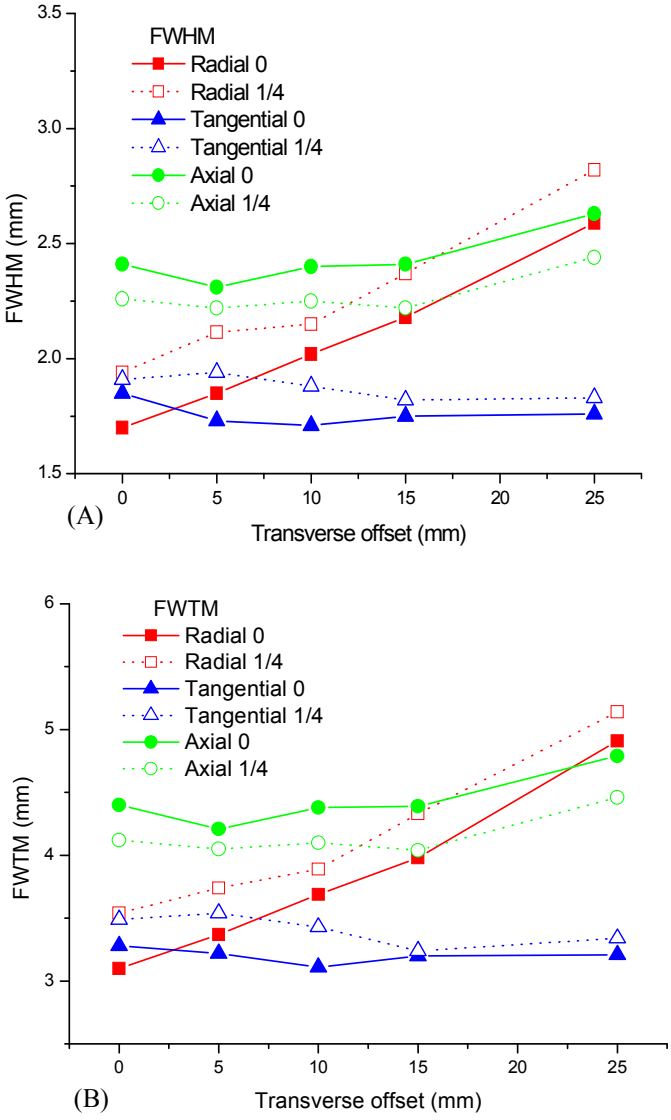

Fig. 1. Radial, tangential and axial spatial resolution as a function of radial offset reported in terms of FWHM (A) and FWTM (B) using FBP reconstruction. Data were measured at two axial positions: at the center of the axial FOV and at ¼ from the center of axial FOV.

B. *Scatter fraction, count losses and random coincidence measurements*

The count rate performance of the scanner for the mouse- and rat-sized phantoms is shown in Fig. 2. The total, true, random, scatter and NEC rates are plotted against the average effective activity concentration for both mouse- and rat-sized phantoms. For the mouse-sized phantom, the peak NECR is 183 kcps at 2.07 MBq/cc whereas the peak true count rate is 320 kcps at 2.50 MBq/cc with a scatter fraction of 19%. The rat-sized phantom produced a scatter fraction of 31 %, with a peak NECR of 67 kcps at 0.23 MBq/cc and a peak true count rate of 186 kcps at 0.27 MBq/cc.

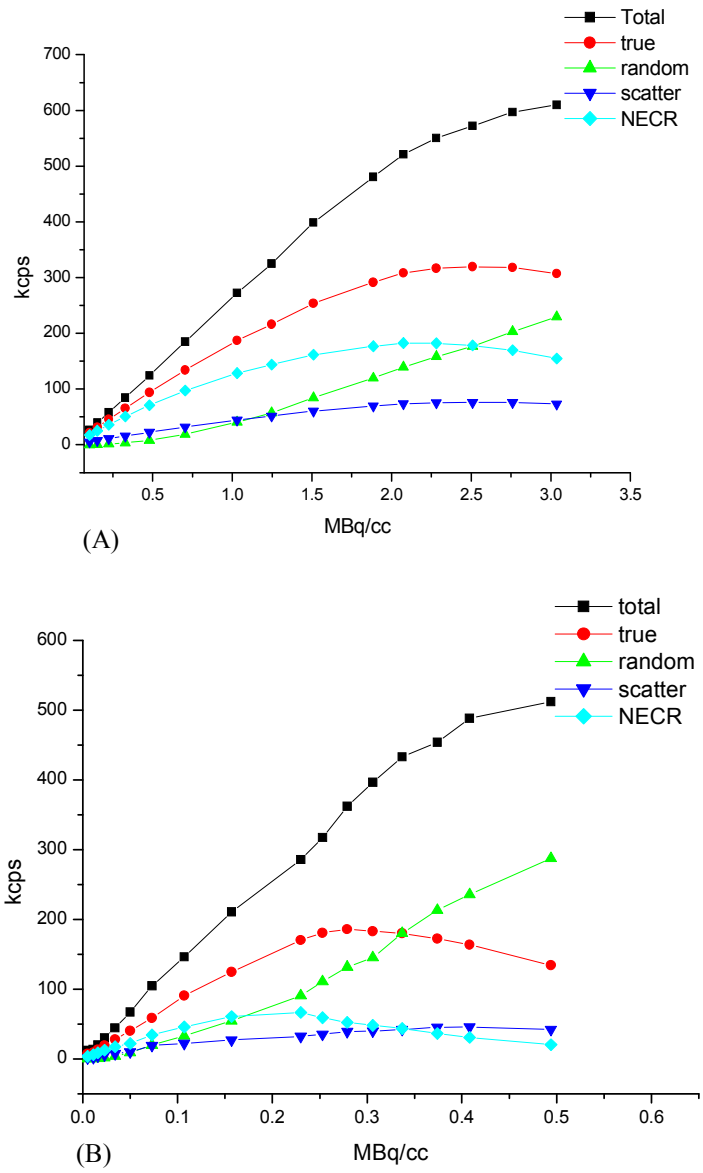

Fig. 2. Count rate performance plots as a function of the average effective activity concentration of the line source for both a mouse-sized phantom (A) and a rat-sized phantom (B).

C. *Sensitivity*

The NEMA NU 4 – 2008 standards suggest calculating the system sensitivity as the sum of the sensitivity for each slice. The total sensitivity for the mouse and rat length is 0.16 cps/Bq whereas the total absolute sensitivity is 12.74%. The system peak absolute sensitivity is 1.33%. Fig. 3A depicts the axial sensitivity profile plotted for the absolute sensitivity S_A against each slice.

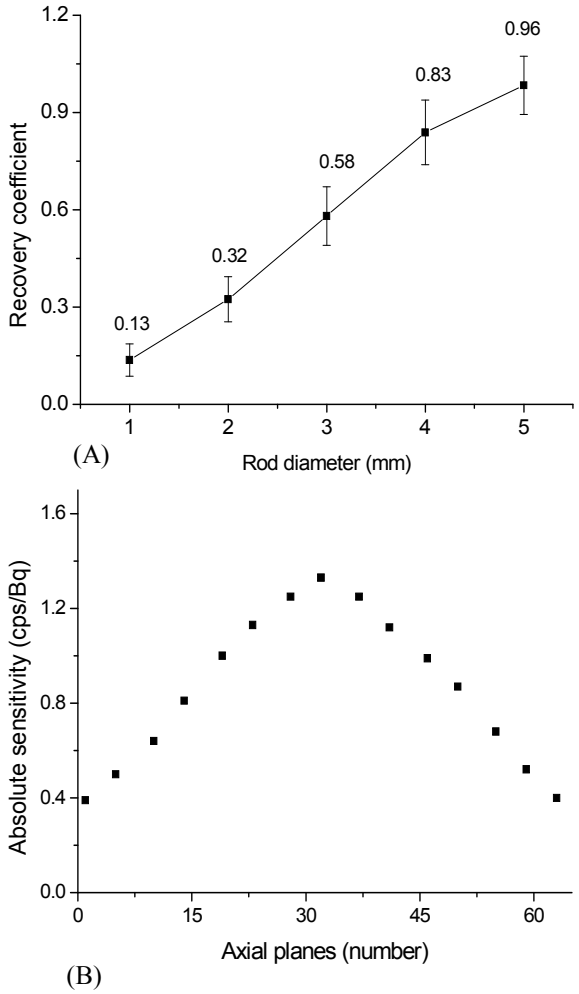

Fig. 3. (A) Recovery coefficients and standard deviations for 5 rods of different size ranging between 1 and 5 mm. (B) The axial absolute sensitivity profile along the z-axis of the LabPET-8™ scanner

D. *Image quality characteristics*

The mean, maximum and minimum activity concentration results and the percentage standard deviation are presented in Table 2. The recovery coefficients (RCs) and absolute standard deviation for the different rods are shown in Fig. 3B.The spill-over ratios and the percentage standard deviation obtained for the water- and air-filled inserts of the image quality phantom are reported in Table 3. Representative images of the NEMA image quality phantom are shown in Fig. 4, illustrating a transaxial view of the 5 rods, a coronal view of NEMA image quality phantom, a transaxial view of the uniform region of the phantom and a profile across the uniform area. The regions of interest defined for quantitative analysis are also shown.

Table 2. Uniformity analysis results obtained using MLEM reconstructions in terms of mean, maximum and minimum activity concentration values in the defined volume of interest (VOI).

Mean (kBq/ml)	Maximum (kBq/ml)	Minimum (kBq/ml)	%STD
126.97	156.35	97.68	7.0 %

Table 3. Spill-over ratios (SOR) and standard deviation (%).

Region	SOR	%STD
Water-filled cylinder	0.20	16.0
Air-filled cylinder	0.11	9.0

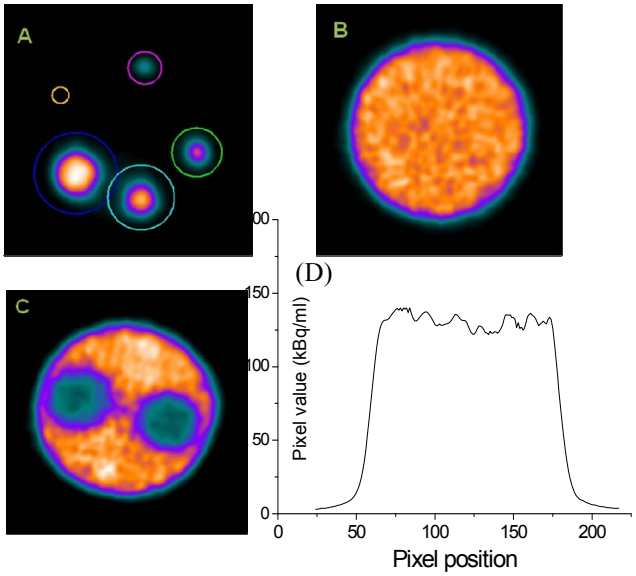

Fig. 4. Images of the NEMA NU-4 image quality phantom showing a transverse plane corresponding to the rods region with ROIs defined on each rod (A), a transverse plane of the uniform region (B), a transverse plane of non-radioactive chambers (C), and a line profile across the uniform area of the phantom (D). The defined ROIs for quantitative analysis are also shown.

IV. DISCUSSION

The overall performance of the LabPET-8™ subsystem of Triumph™ multimodality platform was evaluated according to NEMA NU 4 –2008 standards. Despite that the performance assessment of many small animal PET scanners developed in academic and corporate setting based on the NEMA NU 4 –2008 standards is documented in recent literature [11, 14, 19-24], to the best of our knowledge, there is a lack of published scientific literature reporting on the performance characterization of the LabPET-8™ system using these standards.

The FBP reconstructed spatial resolution shows that the tangential spatial resolution does not vary significantly throughout the transverse FOV. However, the radial resolution is degraded as the radial offset increases. Despite the two-layer scintillation crystal array or phoswich detector to allow coarse estimation of photon depth of interaction, there is a residual transverse parallax error. The deterioration of the axial spatial resolution at higher radial offsets is due to crystal penetration in the axial direction and known limitations of SSRB rebinning used on the LabPET-8™ scanner. In comparison to FBP reconstructed spatial resolution, the MLEM reconstructed spatial resolution which accurately models the physical response of the scanner in the system matrix clearly shows the improvement of the spatial resolution in all three directions. The spatial resolution results for radial and tangential resolutions are in good agreement with those published for the LabPET™ scanner by the University of Sherbrooke group [13]. The slight differences between our and previously published results are due to the difference between acquisition and processing firmware used for generating those results [25], difference in data acquisition energy window (250-650 keV in our case versus 375-650 keV used in the above referenced study) and maximum ring difference applied (31 in our case versus 15). It should also be noted that we neglected in our calculations the effects of the size and shape of the source and non-collinearity of positron annihilation. Fourier rebinning (FORE) should also replace SSRB to improve the axial spatial resolution of the system.

The measured count rate characteristics demonstrate that the LabPET-8™ has suitable count rate performance for optimal imaging of rodents. The achieved NEMA-based peak NECR of 183 kcps for mouse and of 67 kcps for rat-sized phantom is similar to results obtained on the eXplore VISTA small animal PET scanner [26]. The NECR obtained for the rat-sized phantom is lower than the one obtained for the mouse-sized phantom because of the higher photon attenuation of the true events, and higher scatter and random count rates. The NECR for the mouse-sized phantom peaked at a higher activity concentration than for the rat-sized phantom because the true count rate decreases more rapidly than the random count rate as object size increases [27]. The SF values of 19% for the mouse- and 31 % for the rat-sized phantoms for the LabPET-8™ scanner are comparable with those reported for the same system [28] and for the microPET Focus 120 PET scanner [29].

For an energy window of 250-650 keV and timing window of 22 ns, the system peak absolute sensitivity is 1.33% as compared to 2.1% for the LabPET-8™ scanner [13] using multiple coincidence time windows of 10 ns, 15 ns and 20 ns for LYSO-LYSO, LGSO-LYSO and LGSO-LGSO. The discrepancy can be due to different time window settings and the noise threshold which is individually applied to each detector to reject electronic noise. The axial sensitivity profile presents the typical 3D characteristic of axial sensitivities in which a linear drop of sensitivity from the center to the edge of the FOV is observed (Fig. 3A). The NEMA image quality

test provides a common and standardized approach for the overall assessment of image quality of a PET scanner. The %STD which expresses the uniformity of an image is 7% in contrast to 5.29% reported for the Inveon small animal PET scanner [11]. This is due to the fact that our image quality data are not corrected for attenuation and scatter whereas those of the Inveon scanner are corrected for the above mentioned physical degrading factors. The recovery coefficients for the five different rods varied from 0.13 to 0.96. These values are similar to those reported earlier for the LabPET™ scanner [13]. SOR values of water and air-filled chambers are 0.20 and 0.11 having percent standard deviation of 16% and 9%, respectively. Such high values for SOR were expected since the images were not corrected for attenuation and scatter.

Overall, the results demonstrate that the LabPET-8™ subsystem of the Triumph™ multimodality platform is capable of producing high-quality images desirable for molecular imaging-based biomedical research. The performance capabilities of the system can be improved further using fully 3D statistical iterative reconstruction algorithms incorporating accurate modeling of PET scanner response and implementation of CT-based PET quantitative correction procedures.

V. CONCLUSION

The performance of the LabPET-8™ subsystem of the Triumph™ PET/SPECT/CT scanner has been fully characterized using the NEMA NU 04 – 2008 standards. The results indicate that the scanner has a high and uniform spatial resolution across the FOV and a good sensitivity. The count rate performance results demonstrate that the scanner is well suited for imaging rodents allowing the acquisition of good statistics in a relatively short time. The image quality phantom results indicate that the image uniformity and RC values are reasonable. However, these performance parameters can be improved by applying appropriate image correction procedures including CT-based attenuation and scatter corrections [30, 31]. The overall performance shows that the Triumph™ LabPET-8™ scanner is suitable for preclinical imaging-based research and could be considered as one of the most technologically advanced dedicated small-animal PET scanners available today.

ACKNOWLEDGEMENTS

This work was supported by the Swiss National Science Foundation under grant SNSF 3152A0-102143.

REFERENCES

[1] M. E. Phelps, "PET: the merging of biology and imaging into molecular imaging.," *J Nucl Med,* vol. 41, pp. 661-681, 2000.

[2] C. S. Levin and H. Zaidi, "Current trends in preclinical PET system design.," *PET Clinics,* vol. 2, pp. 125-160, 2007/4 2007.

[3] D. B. Stout and H. Zaidi, "Preclinical multimodality imaging in vivo.," *PET Clin,* vol. 3, pp. 251-273, 2008.

[4] K. Ziemons, E. Auffray, R. Barbier, G. Brandenburg, P. Bruyndonckx, Y. Choi, D. Christ, N. Costes, Y. Declais, O. Devroede, and e. al., "The ClearPET™ project: development of a 2nd generation high-performance small animal PET scanner.," *Nucl Instr Meth A,* vol. 537, pp. 307-311, 2005/1/21 2005.

[5] Y.-C. Tai, A. Chatziioannou, Y. Yang, R. W. Silverman, K. Meadors, S. Siegel, D. Newport, J. R. Stickel, and S. Cherry, "MicroPET II: design, development and initial performance of an improved microPET scanner for small-animal imaging.," *Phys Med Biol,* vol. 48, pp. 1519-1537, 2003.

[6] P. M. Bloomfield, S. Rajeswaran, T. J. Spinks, S. P. Hume, R. Myers, S. Ashworth, K. M. Clifford, W. F. Jones, L. G. Byars, J. Young, and et al., "The design and physical characteristics of a small animal positron emission tomograph.," *Phys Med Biol,* vol. 40, pp. 1105-1126, Jun 1995.

[7] A. P. Jeavons, R. A. Chandler, and C. A. R. Dettmar, "A 3D HIDAC-PET camera with sub-millimetre resolution for imaging small animals.," *IEEE Trans Nucl Sci,* vol. 46, pp. 468-473, 1999.

[8] A. Del Guerra, G. Di Domenico, M. Scandola, and G. Zavattini, "YAP-PET: first results of a small animal positron emission tomograph based on YAP:Ce finger crystals.," *IEEE Trans Nucl Sci,* vol. 45, pp. 3105-3108, 1998.

[9] S. Surti, J. S. Karp, A. E. Perkins, R. Freifelder, and G. Muehllehner, "Design evaluation of A-PET: A high sensitivity animal PET camera.," *IEEE Trans Nucl Sci,* vol. 50, pp. 1357-1363, 2003.

[10] Y. C. Tai, A. Ruangma, D. Rowland, S. Siegel, D. F. Newport, P. L. Chow, and R. Laforest, "Performance evaluation of the microPET focus: a third-generation microPET scanner dedicated to animal imaging.," *J Nucl Med,* vol. 46, pp. 455-463, Mar 2005.

[11] Q. Bao, D. Newport, M. Chen, D. B. Stout, and A. F. Chatziioannou, "Performance evaluation of the Inveon dedicated PET preclinical tomograph based on the NEMA NU-4 standards.," *J Nucl Med,* vol. 50, pp. 401-408, March 1, 2009 2009.

[12] S. Xie, R. Ramirez, Y. Liu, T. Xing, J. Uribe, H. Li, Y. Wang, H. Baghaei, S. Kim, and W.-H. Wong, "A pentagon photomultiplier-quadrant-sharing BGO detector for a rodent research PET (RRPET)." *IEEE Trans Nucl Sci,* vol. 52, pp. 210-216, 2005.

[13] M. Bergeron, J. Cadorette, J. F. Beaudoin, M. D. Lepage, G. Robert, V. Selivanov, M. A. Tetrault, N. Viscogliosi, J. P. Norenberg, R. Fontaine, and R. Lecomte, "Performance evaluation of the LabPET APD-based digital PET scanner.," *IEEE Trans Nucl Sci,* vol. 56, pp. 10-16, 2009.

[14] R. Prasad, O. Ratib, and H. Zaidi, "Performance evaluation of the FLEX Triumph™ X-PET scanner using the NEMA NU-04 standards.," *J Nucl Med,* vol. 51, pp. 1608-1615, September 16, 2010 2010.

[15] M. A. Tetrault, N. Viscogliosi, J. Riendeau, F. Belanger, J. B. Michaud, H. Semmaoui, P. Berard, F. Lemieux, L. Arpin, M. Bergeron, J. Cadorette, C. M. Pepin, G. Robert, M. D. Lepage, R. Lecomte, and R. Fontaine, "System architecture of the LabPET small animal PET scanner.," *IEEE Trans Nucl Sci,* vol. 55, pp. 2546-2550, 2008.

[16] National Electrical Manufacturers Association, "NEMA Standards Publication NU 4 – 2008. Performance Measurements of Small Animal Positron Emission Tomographs," National Electrical Manufacturers Association, Rosslyn, VA 2008.

[17] R. Fontaine, F. Belanger, N. Viscogliosi, H. Semmaoui, M. A. Tetrault, J. B. Michaud, C. Pepin, J. Cadorette, and R. Lecomte, "The hardware and signal processing architecture of LabPET™, a small animal APD-based digital PET scanner.," *IEEE Trans Nucl Sci,* vol. 56, pp. 3-9, Feb 2009.

[18] V. V. Selivanov, Y. Picard, J. Cadorette, S. Rodrigue, and R. Lecomte, "Detector response models for statistical iterative image reconstruction in high resolution PET.," *IEEE Trans Nucl Sci,* vol. 47, pp. 1168-1175, 2000.

[19] F. D. Popota, P. Aguiar, Y. Fernandez, C. Lois, D. Pareto, D. Ros, J. Pavia, and J. D. Gispert, "Comparison of NEMA NU 4-2008 vs NEMA NU 2-2001 for the performance evaluation of the microPET R4 system," in *IEEE Nuclear Science Symposium & Medical Imaging Conference*, 25-31 October 2009, Orlando (FL), USA, 2009, pp. 2706-2710.

[20] E. Lage, J. J. Vaquero, A. Sisniega, S. Espana, G. Tapias, M. Abella, A. Rodriguez-Ruano, J. E. Ortuno, A. Udias, and M. Desco, "Design and performance evaluation of a coplanar multimodality scanner for rodent imaging.," *Phys Med Biol,* vol. 54, pp. 5427-5441, Sep 21 2009.

[21] S. A. Kis, I. Lajtos, M. Emri, G. Opposits, T. Bukki, G. Hegyesi, J. Imrek, I. Valastyan, J. Molnar, D. Novak, and L. Balkay, "Performance test of the MiniPET-II small animal scanner according to the NEMA NU-4 standards," in *IEEE Nuclear Science Symposium & Medical Imaging Conference*, 25-31 October 2009, Orlando (FL), USA, 2009, pp. 3185-3189.

[22] M. A. Bahri, A. Plenevaux, G. Warnock, A. Luxen, and A. Seret, "NEMA NU4-2008 image quality performance report for the microPET Focus 120 and for various transmission and reconstruction methods.," *J Nucl Med,* vol. 50, pp. 1730-1738, October 1, 2009 2009.

[23] B. J. Kemp, C. B. Hruska, A. R. McFarland, M. W. Lenox, and V. J. Lowe, "NEMA NU 2-2007 performance measurements of the Siemens Inveon preclinical small animal PET system.," *Phys Med Biol,* vol. 54, pp. 2359-2376, Apr 21 2009.

[24] J. A. Disselhorst, M. Brom, P. Laverman, C. H. Slump, O. C. Boerman, W. J. G. Oyen, M. Gotthardt, and E. P. Visser, "Image-quality assessment for several positron emitters using the NEMA NU 4-2008 standards in the Siemens Inveon small-animal PET scanner.," *J Nucl Med,* vol. 51, pp. 610-617, April 1, 2010 2010.

[25] M. A. Tetrault, M. Bergeron, R. Lecomte, and R. Fontaine, "Firmware upgrade for the data acquisition system of the LabPET small animal PET scanner.," *IEEE Trans Nuc Sci,* vol. 57, pp. 556-560, 2010.

[26] Y. Wang, J. Seidel, B. M. Tsui, J. J. Vaquero, and M. G. Pomper, "Performance evaluation of the GE Healthcare eXplore VISTA dual-ring small-animal PET scanner.," *J Nucl Med,* vol. 47, pp. 1891-1900, Nov 2006.

[27] C. C. Watson, M. E. Casey, B. Bendriem, J. P. Carney, D. W. Townsend, S. Eberl, S. Meikle, and F. P. Difilippo, "Optimizing injected dose in clinical PET by accurately modeling the counting-rate response functions specific to individual patient scans.," *J Nucl Med,* vol. 46, pp. 1825-1834, Nov 2005.

[28] M. Bergeron, J. Cadorette, J.-F. Beaudoin, M.-A. Tetrault, N. Viscogliosi, V. Selivanov, M. D. Lepage, G. Robert, J. P. Norenberg, R. Fontaine, and R. Lecomte, "Imaging performance of the LabPET™ APD-based digital PET scanner," in *IEEE Nuclear Science Symposium Conference Record*, 2008, pp. 3841-3845.

[29] J. S. Kim, J. S. Lee, K. C. Im, S. J. Kim, S.-Y. Kim, D. S. Lee, and D. H. Moon, "Performance measurement of the microPET Focus 120 scanner.," *J Nucl Med,* vol. 48, pp. 1527-1535, September 1, 2007 2007.

[30] R. Prasad, M. R. Ay, O. Ratib, and H. Zaidi, "CT-based attenuation correction on the FLEX Triumph™ preclinical PET/CT scanner.," *IEEE Trans Nucl Sci,* vol. 58, pp. 66-75, 2011.

[31] D. Gutierrez and H. Zaidi, "Assessment of scatter for the micro-CT subsystem of the trimodality FLEX Triumph preclinical scanner.," *Med Phys,* vol. 38, pp. 4154-4165, 2011.